

Galaxy clustering and projected density profiles as traced by satellites in photometric surveys: Methodology and luminosity dependence

Wenting Wang^{1,2}, Y.P. Jing¹, Cheng Li¹, Teppei Okumura^{3,1}, Jiaxin Han^{1,2}

ABSTRACT

We develop a new method which measures the projected density distribution $w_p(r_p)n$ of photometric galaxies surrounding a set of spectroscopically-identified galaxies, and simultaneously the projected cross-correlation function $w_p(r_p)$ between the two populations. In this method we are able to divide the photometric galaxies into luminosity intervals even when redshift information is unavailable, enabling us to measure $w_p(r_p)n$ and $w_p(r_p)$ as a function of not only the luminosity of the spectroscopic galaxy, but also that of the photometric galaxy. We have applied our method to data from the Sloan Digital Sky Survey (SDSS) including a sample of 10^5 luminous red galaxies (LRGs) at $z \sim 0.4$ and a sample of about half a million galaxies at $z \sim 0.1$, both of which are cross-correlated with a deep photometric sample drawn from the SDSS. On large scales, the relative bias factor measured from $w_p(r_p)$ for LRGs at $z \sim 0.4$ depends on luminosity in a manner similar to what is found for galaxies at $z \sim 0.1$, which are usually probed by autocorrelations of spectroscopic samples in previous studies. On scales smaller than a few Mpc and at both $z \sim 0.4$ and $z \sim 0.1$, the $w_p(r_p)n$ and $w_p(r_p)$ for central galaxies with fixed luminosity show quite similar slopes to each other, regardless which types of satellite galaxies we consider. This provides direct support for the assumption commonly-adopted in halo occupation distribution (HOD) models that satellite galaxies of different luminosities are distributed in a similar way, following the dark matter distribution within their host halos.

1. INTRODUCTION

In cold dark matter dominated cosmological models, dark matter halos form in the densest regions in the universe under the influence of gravity, and thus are clustered in a different way from the underlying dark matter. In other words, they are *biased* in spatial distribution relative to dark matter. Since galaxies are believed to form inside these halos, their spatial distribution should also be biased with respect to dark matter. On large scales ($\gtrsim 10\text{Mpc}$), such biasing is

¹Key Laboratory for Research in Galaxies and Cosmology, Shanghai Astronomical Observatory, Chinese Academy of Sciences, Nandan Road 80, Shanghai 200030, China

²Graduate School of the Chinese Academy of Sciences, 19A, Yuquan Road, Beijing, China

³Institute for the Early Universe, Ewha Womans University, Seoul, 120-750, Korea

nearly linear and the clustering of dark matter is also well described by linear perturbation theory. On smaller scales, in contrast, galaxies do not trace dark matter simply. Complicated physical processes involved in galaxy formation and evolution have to be considered if one were to fully understand galaxy clustering. This leads galaxy clustering and biasing to depend on a variety of factors including spatial scale, redshift and galaxy properties. Thus, measuring the clustering of galaxies as a function of their physical properties over large ranges in spatial scale and redshift is helpful for understanding how galaxies have formed and evolved.

Recent large redshift surveys, in particular the Two Degree Field Galaxy Redshift Survey (Colless et al. 2001, 2dFGRS) and the Sloan Digital Sky Survey (York et al. 2000, SDSS), have enabled detailed studies on galaxy clustering in the nearby universe. These studies have well established that the clustering of galaxies depends on a variety of properties, such as luminosity, stellar mass, color, spectral type, and morphology (Norberg et al. 2001, 2002; Madgwick et al. 2003; Zehavi et al. 2002, 2005; Goto et al. 2003; Li et al. 2006; The SDSS Collaboration et al. 2010). More luminous (massive) galaxies are found to cluster more strongly than less luminous (massive) galaxies, with the luminosity (mass) dependence being more remarkable for galaxies brighter than L_* (the characteristic luminosity of the surveys). Moreover, galaxies with redder colors, older stellar populations and more bulge-dominated structure show higher clustering amplitudes and steeper slopes in their two-point correlation functions.

There have also been recent studies on galaxy clustering at higher redshifts. At $z \sim 1$, the DEEP2 Galaxy Redshift Survey (Davis et al. 2003) and the VIMOS-VLT Deep Survey (Le Fèvre et al. 2005, VVDS) have shown that galaxy clustering depends on luminosity, stellar mass, color, spectral type and morphology, largely consistent with what are found for the local universe (Coil et al. 2004, 2006; Meneux et al. 2006; Coil et al. 2008; Meneux et al. 2008; de la Torre et al. 2009). In contrast, the zCOSMOS survey (Lilly et al. 2007) shows no clear luminosity dependence of galaxy clustering over redshift range $0.2 \leq z \leq 1$ (Meneux et al. 2009). More surprisingly, the projected two-point correlation function $w_p(r_p)$ derived from the zCOSMOS is significantly higher and flatter than from the VVDS (Meneux et al. 2008, 2009).

The observational measurements of galaxy clustering at both $z \sim 0$ and $z \sim 1$ as described above have been widely used to test theories of galaxy formation (e.g. Kauffmann et al. 1997; Benson et al. 2000; Li et al. 2007; Guo et al. 2010), as well as to quantify the evolution of galaxy clustering from high to low redshifts (e.g. Zheng et al. 2007; Meneux et al. 2008; Wang & Jing 2010). Galaxy clustering has also been used to constrain halo occupation distribution (HOD) models, which provide statistical description on how galaxies are linked to their host halos and thus useful clues for understanding galaxy formation (e.g., Jing et al. 1998; Jing & Boerner 1998; Peacock & Smith 2000; Ma & Fry 2000; Seljak 2000; Scoccimarro et al. 2001; Berlind & Weinberg 2002; Cooray & Sheth 2002; Yang et al. 2003; Zheng et al. 2005; Tinker et al. 2005).

At intermediate redshifts ($0.2 \lesssim z \lesssim 1$), progress on measuring galaxy clustering has been relatively hampered by the lack of suitable data sets. A few studies (e.g. Shepherd et al. 2001;

Carlberg et al. 2001; Firth et al. 2002; Phleps et al. 2006) have measured galaxy clustering as a function of color which are in broad agreement with results found for the local universe. However, the dependence of clustering on luminosity, which is well seen in the local universe, has not been fully established at these intermediate redshifts, very likely due to the limited size of the spectroscopic samples. These samples usually cover too small area on the sky and so suffer from both sampling noise and large-scale structure noise (the so-called *cosmic variance* effect).

In this paper we develop a new method for estimating the projected two-point correlation function $w_p(r_p)$ for a given set of spectroscopically identified galaxies (hereafter *main* galaxies⁴). Rather than measuring the *autocorrelation* of these galaxies as in most previous studies, we opt to cross correlate our galaxies with a large sample of photometric galaxies (hereafter *satellite* galaxies). In brief, we first determine the projected, average number density distribution $w_p(r_p)n$ of the satellites surrounding the main galaxies, from which we then estimate the projected two-point correlation function $w_p(r_p)$. The photometric sample is usually the parent sample of the main galaxies, but goes to much fainter limiting magnitudes. The main galaxies could be clusters (or groups) of galaxies, central galaxies of dark matter halos such as the luminous red galaxies (LRGs) in the SDSS, quasars, or any spectroscopic galaxy samples of interest. Our method can yield a measurement of the projected density distribution of galaxies with certain physical properties (such as luminosity, color, etc.) around spectroscopic objects of certain properties.

Previous studies of satellite galaxy distribution around bright objects are mostly limited to low redshifts (e.g. Lake & Tremaine 1980; Phillipps & Shanks 1987; Vader & Sandage 1991; Lorrimer et al. 1994; Sales & Lambas 2005; Chen et al. 2006). Here we apply our method to a deep, photometric galaxy catalogue and a spectroscopic LRG sample at intermediate redshifts ($z \sim 0.4$), both of which are drawn from the final data release of the SDSS, in order to estimate $w_p(r_p)n$, the projected density distribution of galaxies around central LRGs. By calculating analytically the galaxy number density n using the luminosity function provided by Blanton et al. (2003) (hereafter B03) and the E -evolution model of Faber et al. (2007) (here after F07), we further obtain the projected cross-correlation function $w_p(r_p)$ between the two populations. On scales smaller than a few Mpc, this statistic yields the density distribution of galaxies in dark matter halos around their central galaxies. On larger scales, this measures the linear bias factor of galaxies at $z \sim 0.4$. For the first time we show that the luminosity dependence of galaxy clustering at this redshift is very similar to that observed in the local universe. Similarly, we have also measured the projected density profiles and projected cross correlations for the SDSS spectroscopic Main galaxy sample (median redshift $z \sim 0.1$) using the same methodology and the same photometric sample. Comparing our results at the two redshifts, we discuss the evolution of galaxy clustering from $z \sim 0.4$ to the present day.

We describe our galaxy catalogues in § 2. We then introduce in detail our method of obtaining $w_p(r_p)n$ and how to divide luminosity subsamples for the photometric catalogue when redshift

⁴Not confused with SDSS Main sample galaxies at local universe.

information is unavailable. We apply our method to SDSS data and show the results in § 4. We summarize our study in the last section. Throughout this paper we assume a cosmology with $\Omega_m = 0.3, \Omega_\Lambda = 0.7$ and $H_0 = 100 h \text{ km s}^{-1} \text{ Mpc}^{-1}$ ($h = 1$).

2. Data

2.1. The LRG sample at intermediate redshift

The LRG sample is constructed from the SDSS data release 7 (DR7 Abazajian et al. 2009), consisting of 101,658 objects with spectroscopically measured redshift in the range $0.16 < z < 0.47$, absolute magnitude limited to $-23.2 < M_{0.3g} < -21.2$ and redshift confidence parameter greater than 0.95. Here $M_{0.3g}$ is the g -band absolute magnitude K - and E -corrected to redshift $z = 0.3$ (see Eisenstein et al. 2001 for references). We further select those LRGs that are expected to be the central galaxy of their host dark matter halos, using a method similar to that adopted in Reid & Spergel (2009) and Okumura et al. (2009). In particular, we use linking lengths of $0.8 h^{-1} \text{ Mpc}$ and $20 h^{-1} \text{ Mpc}$ for separations perpendicular and parallel to the line of sight when linking galaxies into groups. This leads to a total of 93802 central galaxies (about 92.3% of the initial LRG catalogue), covering a sky area pretty the same as that of Kazin et al. (2010). From this catalogue we select five samples by dividing all the galaxies into two luminosity intervals, which are $-23.2 < M_{0.3g} < -21.8$ and $-21.8 < M_{0.3g} < -21.2$, as well as three redshift intervals, which are $0.16 < z < 0.26$, $0.26 < z < 0.36$ and $0.36 < z < 0.46$. These samples so selected are volume limited, except **Sample L4** which is approximately, but not perfectly volume limited as can be seen from fig. 1 of Zehavi et al. (2005). Details of our samples are listed in Table 1. Figure 1 shows the redshift distributions of our LRGs in the two luminosity intervals.

2.2. The low-redshift galaxy sample

Our spectroscopic galaxy sample in the local Universe is constructed from the New York University Value Added Galaxy Catalog (NYU-VAGC)⁵, which is built by Blanton et al. (2005) based on the SDSS DR7. From the NYU-VAGC we select a magnitude-limited sample of 533,731 objects with $0.001 < z < 0.5$ and r -band Petrosian magnitude in the range $10.0 < r < 17.6$. The sample has a median redshift of $z = 0.09$, with the majority of the galaxies at $z < 0.25$. The galaxies are divided into five non-overlapping redshift bins, ranging from $z = 0.03$ to $z = 0.23$ with an equal interval of $\Delta z = 0.04$. The galaxies in each redshift bin are further restricted to various luminosity ranges, giving rise to a set of eight volume limited samples as listed in Table 2. The r -band absolute magnitude $M_{0.1r}$ is K - and E -corrected to its value at $z = 0.1$ following B03. Figure 2 shows the redshift distribution of the galaxies falling into the three luminosity cuts

⁵<http://sdss.physics.nyu.edu/vagc/>

which are used to select the samples. These samples by construction are at lower redshifts when compared to the LRG samples, allowing us to make use of photometric galaxies for our analysis over wide ranges in luminosity and redshift. We don't attempt to select central galaxies as done for LRGs above, as it is not straightforward to do so. Thus one should keep in mind that by using the low-redshift samples selected here we will measure density profiles and projected correlations for general populations of galaxies, not only centrals.

2.3. The photometric galaxy sample and random samples

We construct our photometric galaxy sample from the `datasweep` catalogue which is included as a part of the NYU-VAGC. This is a compressed version of the full photometric catalogue of the SDSS DR7 that was used by Blanton et al. (2005) to build the NYU-VAGC. Starting from the `datasweep` catalogue, we select all galaxies with r -band apparent model magnitudes in the range $10 < r < 21$ after a correction for Galactic extinction, and point spread function and model fluxes satisfying $f_{model} > 0.875 \times f_{PSF}$ in all five bands. In order to select unique objects in a run that are not at the edge of the field, we require the `RUN PRIMARY` flag to be set and the `RUN EDGE` flag not to be set. Finally we also require the galaxies to be located within *target tiles* of the Legacy Survey (Blanton et al. 2003). This procedure results in a sample of ~ 25.5 million galaxies.

As shown by Ross et al. (2007), the `datasweep` catalogue needs to be properly masked, otherwise the angular correlation function obtained would be falsely flat on large scales. We describe the SDSS imaging geometry in terms of disjoint spherical polygons (Hamilton & Tegmark 2002; Tegmark et al. 2002; Blanton et al. 2005), which accompany the NYU-VAGC release and are available from the NYU-VAGC website. We exclude all polygons (and thus the galaxies located within them) which contain any object with seeing greater than $1.5''$ or Galactic extinction $A_r > 0.2$. We also exclude polygons that intersect the mask for galaxy M101 as described in Ross et al. (2007). As a result, a fraction of about 14.32% of the total survey area has been discarded, slightly larger than in Ross et al. (2007) where the authors exclude image pixels rather than polygons with less strict criteria than adopted here. We also restrict ourselves to galaxies located in the main contiguous area of the survey in the northern Galactic cap, excluding the three survey strips in the southern cap (about 10 per cent of the full survey area). These restrictions result in a final sample of ~ 19.7 million galaxies.

We have constructed a random sample which has exactly the same geometry and limiting magnitudes as the real photometric sample. This is done by generating points at random within the polygons covering the real galaxies.

3. Methodology

In our method we estimate in the first place the angular cross correlation function $w(\theta)$ between a given set of main galaxies selected by luminosity and redshift (samples listed in Tables 1 and 2) and a set of satellite galaxies in a given luminosity range selected from the photometric sample. Next, we convert $w(\theta)$ to determine the projected density distribution $w_p(r_p)n$ of the satellite galaxies around the main galaxies, from which we finally estimate the projected cross correlation function $w_p(r_p)$ between the two populations. In this section we first describe how we select satellite galaxies from the photometric sample for a given luminosity range, followed by detailed description of our measures of angular correlation functions as well as the way of determining $w_p(r_p)n$ and $w_p(r_p)$.

3.1. Selecting photometric galaxies according to luminosity and redshift

Considering a sample of main galaxies with absolute magnitude and redshift in the ranges $M_{main,1} < M_{main} < M_{main,2}$ and $z_1 < z_{main} < z_2$, we want to measure the cross-correlation of this sample with a set of satellite galaxies with absolute magnitude limited to $M_{sat,1} < M_{sat} < M_{sat,2}$. Due to the lack of redshift information for the photometric sample, it is not straightforward to determine which galaxies should be selected in order to have a subset falling in the expected luminosity range. To overcome this difficulty, we assume that the cross-correlation signal is dominated by those satellites that are at the same redshifts as the main galaxies, while both the foreground (below z_1) and the background (above z_2) galaxies contribute little to the signal. This is reasonably true when the redshift interval $z_2 - z_1$ in consideration is small enough, as the clustering power of galaxies decreases rapidly with increasing separation. Thus, when estimating the angular correlation function, we restrict ourselves to satellite galaxies with apparent magnitude $m_{sat,1} < m_{sat} < m_{sat,2}$, which is the magnitude range for satellite galaxies to have $M_{sat,1} < M_{sat} < M_{sat,2}$ at $z_1 < z_{sat} < z_2$.

When calculating the apparent magnitude for a given absolute magnitude and redshift, we have adopted the empirical formula of K -correction presented by Westra et al. (2010), which works at r -band as a function of observed $g - r$ color and redshift. Since K -correction value changes slowly with redshift, we adopt $(z_1 + z_2)/2$ as the input redshift value when applying the formula for simplicity. In this paper we adopt the $^{0.1}r$ -band luminosity function from B03, and so we convert the apparent magnitude in r to that in $^{0.1}r$ using the analytical conversion formula provided by Blanton & Roweis (2007).

3.2. Measuring angular correlation functions

We use two estimators to measure the angular cross correlation function between a spectroscopic sample of main galaxies and a photometric sample of satellites. For small separations

($\theta \lesssim 1000''$) we use the standard estimator (Davis & Peebles 1983)

$$w(\theta) = \frac{QD(\theta)}{QR(\theta)} - 1, \quad (1)$$

where θ is the angular separation, and $QD(\theta)$ and $QR(\theta)$ are the cross pair counts between the spectroscopic sample and the photometric sample, and between the same spectroscopic sample and the random sample. Note that QR is normalized according to the ratio of the size of the photometric and random samples. For separations larger than $\theta \sim 1000''$, we instead use a Hamilton-like estimator (Hamilton 1993)

$$w(\theta) = \frac{QD(\theta)RR(\theta)}{QR(\theta)DR(\theta)} - 1, \quad (2)$$

where RR is the pair count of the random sample, and DR the cross pair count between the photometric and random samples. This estimator is expected to work better on large scales than the standard one, since it is less sensitive to the uncertainties in the mean number density of photometric galaxies (Hamilton 1993). The two estimators are almost identical on small scales. In order to reduce computation time, we apply the standard estimator onto a random sample of 30 million points for separations $\theta \lesssim 1000''$, while a smaller sample of 0.9 million random points and the Hamilton-line estimator are used for larger separations.

3.3. Converting $w(\theta)$ to $w_p(r_p)n$ and $w(r_p)$

Given a measurement of $w(\theta)$ we estimate the corresponding projected correlation function $w_p(r_p)$ and/or projected density profile $w_p(r_p)n$ in the following two ways. In this subsection the photometric (satellite galaxies) and main (spectroscopic galaxies) samples used to estimate these statistics are named **sample 1** and **sample 2**.

3.3.1. Direct conversion from $w(\theta)$ to $w_p(r_p)$

The relation between angular correlation function $w(\theta)$ and real space correlation function $\xi(r)$ is (see Peebles 1980)

$$w(\theta) = \frac{\int_0^\infty x_1^2 x_2^2 dx_1 dx_2 a_1^3 a_2^3 n_1 n_2 \xi(r_{1,2})}{\mathcal{N}_1 \mathcal{N}_2}, \quad (3)$$

where a and x stands for scale factor and comoving distance respectively; $r_{1,2}$ is the real space separation between sample 1 and sample 2 galaxies; \mathcal{N}_1 and \mathcal{N}_2 are the surface number densities of Sample 1 and 2; n_1 and n_2 are comoving spatial number densities for the two samples. Taking n_2 as a summation of Dirac delta functions, we have

$$n_2 = \sum_k \delta(\vec{r}_2 - \vec{r}_k), \quad (4)$$

where vector r_k stands for galaxy positions in Sample 2. Thus Eqn. (3) becomes

$$w(\theta) = \frac{\Omega_1 \Omega_2 \sum_k \int_0^\infty x_1^2 x_2^2 dx_1 dx_2 a_1^3 a_2^3 n_1 \delta(\vec{r}_2 - \vec{r}_k) \xi(r_{1,2})}{N_1 N_2} \quad (5)$$

$$= \frac{\Omega_1 \sum_k \int_0^\infty x_1^2 dx_1 a_1^3 n_1 \xi(r_{1,k})}{N_1 N_2} \quad (6)$$

$$= \frac{\sum_k \int_0^\infty dN_1/dz_1 \xi(r_{1,k}) dz_1}{N_1 N_2}, \quad (7)$$

where

$$r_{1,k} = \sqrt{r_1^2 + r_k^2 - 2r_1 r_k \cos(\theta)}, \quad (8)$$

and r_1 and r_k are the comoving distances for galaxies in sample 1 and the k th galaxy in sample 2. Here N_1 and N_2 are the total number of objects in the two samples. Let N_k denote the number of galaxies with approximately the same distance r_k (or redshift z_k) in sample 2, then Eqn. (7) can be written as

$$w(\theta) = \frac{\sum_k N_k \int_0^\infty dN_1/dz_1 \xi(r_{1,k}) dz_1}{N_1 N_2}. \quad (9)$$

If the redshift bin of sample 2 is thin enough, all the galaxies within it can be regarded as at the same redshift. This gives rise to a much simplified relation between $w(\theta)$ and $\xi(r)$:

$$w(\theta) = \frac{\int_0^\infty dN_1/dz_1 \xi(r_{1,2}) dz_1}{N_1}. \quad (10)$$

On the other hand, the relation between $w_p(r_p)$ and $\xi(r)$ is known to be

$$w_p(r_p) = 2 \int_{r_p}^\infty \xi(r) \frac{r dr}{\sqrt{r^2 - r_p^2}} = \int_{z_l}^{z_u} \xi(r_{1,2}) \frac{dD}{dz_1} dz_1, \quad (11)$$

where D is the comoving distance of sample 1 galaxy, r_p the projected physical separation, z_l and z_u the lower and upper limits of the redshift interval in consideration. If the change of dN_1/dz_1 and dD/dz_1 with redshift is much slower compared with that of $\xi(r_{1,k})$ as a function of $r_{1,k}$, where $r_{1,k}$ depends on z_1 , we can take dN_1/dz_1 and dD/dz_1 out of the integral. Thus for a thin redshift bin the ratio between $w(\theta)$ and $w_p(r_p)$ is simply approximated by

$$\frac{w(\theta)}{w_p(r_p)} = \frac{dN_1/dz_1}{N_1 dD/dz_1} \bigg|_{z_1=z_{med}}, \quad (12)$$

where $r_p = 2D \sin(\frac{\theta}{2})$ and z_{med} is the median of the redshift bin. In practice we instead calculate the ratio in the following way to take into account the redshift dependence (though very weak) of dN_1/dz_1 and dD/dz_1 :

$$\frac{w(\theta)}{w_p(r_p)} = \frac{\int_{z_l}^{z_u} \left(\frac{dN_1/dz_1}{N_1 dD/dz_1} \bigg|_{z_1=z} \right) (dN_2/dz) dz}{\int_{z_l}^{z_u} (dN_2/dz) dz}. \quad (13)$$

Quantities in the right side of Eqn. (13) can be obtained from data catalogue directly (N_2 and dN_2/dz) or from the luminosity function analytically (dN_1/dz), and we can then use Eqn. (13) to convert $w(\theta)$ to $w_p(r_p)$.

In order to see to what extent this approximation holds, we do a test as follows. We first calculate the linear transfer function using CMBfast code (Seljak & Zaldarriaga 1996; Zaldarriaga et al. 1998; Zaldarriaga & Seljak 2000). We then calculate nonlinear power spectrum $P_{nl}(k)$ from the linear one $P_l(k)$ following Peacock & Dodds (1996). The real-space correlation function $\xi(r)$ is then obtained by Fourier transforming $P_{nl}(k)$. The amplitude of $\xi(r)$ is arbitrarily given which has no effect on the ratio between $w(\theta)$ and $w_p(r_p)$. Next, the redshift distribution dN_1/dz_1 for a certain magnitude bin of sample 1 galaxies is calculated analytically from the luminosity function of B03. Using Eqn. (9) and (11) we determine $w(\theta)$ and $w_p(r_p)$ for this magnitude bin, and thus the *true* value of their ratio which we denote as $ratio_{true}$. When integrating the right part of Eqn. (9) we fix r_p and let the binning of θ vary accordingly. We also calculate an approximated value for the same ratio using Eqn. (13), which we denote as $ratio_{analy}$ and compare to the true ratio in order to test the validity of Eqn. (13).

Figure 3 shows the relative difference in the $w(\theta)/w_p(r_p)$ ratio between the approximated and the true values, $(ratio_{analy} - ratio_{true})/ratio_{true}$, for sample 2 galaxies with $0.07 < z_2 < 0.078$ and $-23.0 < M_2 < -21.0$, and sample 1 galaxies in different absolute magnitude intervals (as indicated in each panel). The approximated ratio agrees pretty well with the true value, at 1% accuracy or better, for separations $r_p \lesssim 10$ Mpc and for all luminosities considered. The discrepancy increases at larger separations, but well below 3% level even at the largest scale probed here (~ 30 Mpc), which mainly comes from the distant-observer approximation adopted here. The accuracy of Eqn. (13) is expected to be higher for higher redshifts where the distant-observer approximation works better. We thus conclude that our approximation in Eqn. (13) works at substantially high accuracies for our purpose.

3.3.2. Indirect conversion through $w_p(r_p)n$

We propose a second method here for estimating $w_p(r_p)$. Rather than directly converting $w(\theta)$ to $w_p(r_p)$, we first convert the former to a projected density profile $w_p(r_p)n_1$, from which we then estimate $w_p(r_p)$ by calculating analytically the spatial number density n_1 from the luminosity function. $w_p(r_p)n_1$ is obtained as a byproduct without suffering from uncertainties in galaxy luminosity function.

In this method we estimate a *weighted* angular correlation function $w(\theta)_{weight}$ instead of the traditional function $w(\theta)$ as discussed above. This is measured using the same estimators given in Eqn. (1) and (2), except that each spectroscopic galaxy in sample 2 is weighted by D^{-2} , inverse of the square of comoving distance of sample 2 galaxies. It can be easily proved using Eqn. (13) that for a thin redshift interval of the spectroscopic sample (sample 2), $N_1 w(\theta)_{weight}/\Omega$ essentially

equals to the projected density profile $w_p(r_p)n_1$, i.e.,

$$w_p(r_p)n_1 = \frac{N_1 w(\theta)_{weight}}{\Omega}, \quad (14)$$

where N_1 and n_1 are the number and number density of photometric galaxies (sample 1), and Ω the total sky coverage of sample 1. Given the projected density profile $w_p(r_p)n_1$ estimated by Eqn. (14) as well as the spatial number density of galaxies n_1 analytically calculated from the luminosity function, we finally estimate the projected correlation function $w_p(r_p)$ by dividing $w_p(r_p)n_1$ by n_1 . We emphasize here the projected density profile $w_p(r_p)n_1$ does not suffer from uncertainties in luminosity function, because all quantities in the right side of Eqn. (14) can be obtained from data.

To calculate n_1 , we adopt the luminosity evolution model and the luminosity function at $z = 0.1$ from B03 when doing calculation for spectroscopic galaxies at low redshifts (samples selected from the SDSS Main galaxy catalogue as listed in Table 2). Considering that the evolution model of B03 is based on low-redshift data ($z \lesssim 0.25$), which might not be suitable for higher redshifts, we adopt the evolution model of F07 for our LRG samples. Moreover, we need to convert the F07 model from B -band to the $^{0.1}r$ -band at which our galaxies are observed. Assuming that the slope of the luminosity evolution doesn't depend on waveband, we obtain the $^{0.1}r$ -band luminosity evolution model by simply shifting the amplitude of the B -band model from F07 so as to have an amplitude at $z = 0.1$ which equals to the amplitude of the $^{0.1}r$ -band model of B03. In this manner the slopes of the two models remain unmodified, which are $Q = -1.23$ for F07 and -1.62 for B03 respectively (see their papers for details).

In conclusion, the projected cross-correlation function $w_p(r_p)$ can be measured either from Eqn. (13) by direct conversion of $w(\theta)$, or from Eqn. (14) by indirect conversion through estimating $w_p(r_p)n$. After having made extensive comparisons, we found that the two methods give rise to almost identical results. In what follows we choose to use the second method only, and it simultaneously provides both $w_p(r_p)$ as $w_p(r_p)n$.

3.4. Division and combination of redshift subsamples

Before going to the next section where we apply our method to the SDSS samples, we have to address an important issue which we have ignored so far. As mentioned above, our method for selecting photometric galaxies according to luminosity and redshift is valid only when the redshift interval $z_2 - z_1$ is small enough. However, the redshift intervals used to select our spectroscopic galaxy samples apparently do not satisfy this condition. Our solution is to further divide the galaxies in a given spectroscopic sample into a number of subsamples which are equally spaced in redshift (hereafter called redshift sub-shells). See Tables 1 and 2 for the number of redshift sub-shells adopted for our samples. For a given sample, we measure the weighted angular cross-correlation function $w(\theta)_{weight}$ (see above) for each sub-shell separately by cross-correlating it with

satellites selected from the photometric catalogue in the way described above according to the expected luminosity range and the redshift range of the sub-shell. Each $w(\theta)_{weight}$ measurement is then converted to give the corresponding projected density profile $w_p(r_p)n$ as well as the projected cross-correlation function $w_p(r_p)$, using the second method described above. Estimates of these quantities for the sub-shells are then averaged to give the results for their parent sample as a whole. In this procedure each sub-shell is weighted by V_i/σ_i^2 , with V_i being the comoving volume covered by the i th sub-shell and σ_i the variance of $w_p(r_p)n$ or $w_p(r_p)$ of the sub-shell. In order to estimate σ_i we have generated 100 bootstrap samples for each sub-shell. The variance σ_i of a sub-shell is then estimated by the $1-\sigma$ scatter between all its bootstrap samples. This weighting scheme ensures the averaged $w_p(r_p)n$ or $w_p(r_p)$ to be determined largely by sub-shells with relatively large volume and high signal-to-noise ratio (S/N) measurements, thus effectively reducing the overall sampling noise and cosmic variance.

In order to increase the accuracy of our method, one may want to increase the number of sub-shells for a given redshift range, but at the cost of increasing both the sampling noise and the large-scale structure noise (the *cosmic variance*). In practice, we split a spectroscopic sample into redshift sub-shells by requiring $\Delta z/z \lesssim 0.1$, where Δz is the thickness of the sub-shells and z is the mean redshift of the sample. With this restriction the difference between $m_2 - m_1$ and $M_2 - M_1$ ranges from ~ 0.25 occurring for several low-redshift sub-shells to ~ 0.1 at best. Extensive tests show that our results are robust to reasonable change of the thickness of sub-shells. For instance, taking **Sample L1** from Table 1 as the spectroscopic sample, the cross-correlation function measured by 10 sub-shells differs from that by 5 sub-shells by at most 10% for photometric galaxies with $-22 < M < -21.5$, and by only about 3% for the faintest luminosity bin $-19.5 < M < -19.0$.

3.5. Error estimation

We estimate the error in the averaged $w_p(r_p)n$ or $w_p(r_p)$ by

$$\Delta = \begin{cases} \sqrt{\sigma^2 \times \frac{\chi^2}{\text{dof.}}} & \text{if } \frac{\chi^2}{\text{dof.}} > 1 \\ \sigma & \text{if } \frac{\chi^2}{\text{dof.}} \leq 1, \end{cases} \quad (15)$$

with

$$\sigma^2 = \sum_{i=1}^{N_{sub}} \frac{V_i^2}{\sigma_i^2} \bigg/ \left(\sum_{i=1}^{N_{sub}} \frac{V_i}{\sigma_i^2} \right)^2, \quad (16)$$

$$\chi^2/\text{dof.} = \frac{1}{N_{sub} - 1} \sum_{i=1}^{N_{sub}} (x_i - x_{avg})^2 \sigma_i^{-2}, \quad (17)$$

where the sum goes over all the sub-shells of a given spectroscopic sample; x_i is the measurement of $w_p(r_p)n$ or $w_p(r_p)$ of the i th sub-shell and x_{avg} the average measurement for all the sub-shells

as a whole; N_{sub} is the number of sub-shells. Overall, Eqn. (15) should be able to include both the volume effect (through factor V_i) and the sampling noise (through σ_i), thus providing a reasonable estimate of the errors in our measurements. By weighting the error by $\sqrt{\frac{\chi^2}{\text{dof}}}$, we mean to take into account the large variation from sub-shell to sub-shell in some cases.

To better understand the error contribution from different redshift sub-shells, we plot in Figure 4 the $w_p(r_p)$ measurements for **Sample L1** listed in Table 1. Different panels correspond for satellite galaxies in different luminosity intervals. In each panel, we plot $w_p(r_p)$ for all the five sub-shells with their redshift ranges indicated in the bottom-right panel. Error bars on the $w_p(r_p)$ curves are estimated using the bootstrap resampling technique, i.e. σ_i in Eqn. (16) and (17). We see that at fixed satellite luminosity, $w_p(r_p)$ measurements of different sub-shells are almost on top of each other, indicating that the scatter between sub-shells is fairly small. This again shows that the correlation functions measured with our method are insensitive to the number of redshift sub-shells.

We note that the overall error increases rapidly with luminosity at the bright end. This reflects not only the sampling noise of the small samples, but more importantly, also an effect of a huge foreground population which significantly suppresses the cross-correlation signals. Letting $w'(\theta)$ be the angular correlation function between a spectroscopic sample with $z_1 < z < z_2$ and a photometric sample including galaxies of all redshifts, and $w(\theta)$ the one between the same spectroscopic sample and a sample of photometric galaxies covering redshift range $z_1 < z < z_2$, one can easily show that

$$w'(\theta) = \frac{N_{GS}}{N_G} w(\theta), \quad (18)$$

where N_G and N_{GS} are respectively the number of photometric galaxies in the full sample and in the redshift range $z_1 < z < z_2$. In this case the estimated correlation signal is suppressed by a factor of $\frac{N_{GS}}{N_G}$, a large effect in particular when $N_G \gg N_{GS}$ as in bright samples.

This is explained more clearly in Figure 5 where we plot the redshift distribution as calculated using the luminosity function of B03 for photometric galaxies which are selected according to luminosity and redshift using the method described in § 3.1. Plotted in different lines are the distributions for different luminosity ranges with redshift range fixed to $0.2 < z < 0.22$. According to our method of dividing photometric sample into luminosity subsamples, photometric galaxies selected to serve our purpose of a certain luminosity bin have the desired luminosity at the chosen redshift. As can be seen from the figure, in the brightest luminosity interval ($-22.5 < M_{0.1r} < -22.0$, solid line) only a small fraction of the galaxies are located within the expected redshift range, where the majority of galaxies are intrinsically fainter. It is this population that suppresses the cross-correlations that we measure at the bright end, leading to large uncertainties as seen in Figure 4.

4. Applications to SDSS galaxies

4.1. Projected cross-correlations and density profiles of LRGs

In Figure 6 we show projected density profile $w_p(r_p)n$ for LRGs in different intervals of luminosity and redshift, as traced by satellite galaxies of different luminosities. Results are plotted for LRGs with $-23.2 < M_{0.3g} < -21.8$ in panels on the left and for those with $-21.8 < M_{0.3g} < -21.2$ on the right, with panels from top to bottom corresponding to different redshift bins. The $w_p(r_p)n$ traced by satellites in different luminosity ranges are shown using different lines as indicated in the bottom-right panel. As can be seen from the figure, the projected number density of satellites around central LRGs decreases as the luminosity of satellites increases. This is true for all redshifts and scales probed here. In particular, such luminosity dependence is weak for satellites fainter than the characteristic luminosity of the Schechter luminosity function ($M_{0.1r} = -20.44$ for the SDSS), and becomes remarkable for brighter satellites. The change of the amplitude mainly reflects the number density of galaxies as a function of their luminosity. From the figure one can easily read out the number of galaxies in the host halos of the LRGs. For example, on average there are about 3 galaxies of $-20.5 < M < -20$ in the host halo of a LRG in **Sample L1**, assuming the host halo radius is $0.3h^{-1}\text{Mpc}$.

In Figure 7 we show projected cross-correlation function $w_p(r_p)$ obtained from the $w_p(r_p)n$ measurements shown in Figure 6, for the same set of LRG samples and the same intervals of satellite luminosity. At fixed scale and redshift, the amplitude of $w_p(r_p)$ increases with increasing luminosity, a trend which has already been well established by previous studies. It is interesting to see from both figures that, although $w_p(r_p)n$ and $w_p(r_p)$ both show systematic trends with satellite luminosity in amplitude, their slope remains fairly universal for given redshift and fixed central galaxy luminosity, regardless which types of satellites we consider. This provides direct observational evidence that satellite galaxies of different luminosities follow the distribution of dark matter in the same way within their dark matter halos, an assumption adopted in many previous studies on HOD modelling of galaxy distribution.

In Figure 8 we plot the $w_p(r_p)$ again in order to explore the evolution with redshift. Measurements of different satellite luminosities are shown in different panels, while in each panel we compare $w_p(r_p)$ measured at different redshifts for fixed luminosity. Note that in this figure we have considered the luminosity evolution of galaxies, as we aim to study how the projected density distribution and cross-correlation around the LRGs have evolved over the redshift range probed. We do not include E -correction in Figures 4,6 and 7, because we want the results there to be less affected by possible uncertainty in the luminosity evolution model. From Figure 8, we see significant increase in the amplitude of $w_p(r_p)$ as redshift goes from $z = 0.4$ to 0.2 . Taking the $-21.0 < M < -20.5$ bin in the left column for example, on average the $w_p(r_p)$ amplitude differs by a factor of about 2 between the result of $z \sim 0.2$ (blue curve) and $z \sim 0.4$ (green curve) at separations $r_p < 0.3h^{-1}\text{Mpc}$, the typical boundary of LRG host halos.

It is important to understand whether the significant evolution seen above could be explained purely by evolution in dark matter distribution, or additional processes related to galaxies themselves are necessary. To the end we have done a simple calculation as follows. We assume that there is no merger occurring between galaxies or between their host halos. In this case all galaxies and halos have been evolving in a passive manner, and the total number of each keeps unchanged during the period in consideration. Thus galaxies at different redshifts are the same population which are hosted by the same set of halos. We calculate a dark matter density profile averaged over all dark matter halos that are expected to host LRGs of given redshift and luminosity, by

$$\rho_{avg}(r) = \frac{\int_{M_{min}}^{M_{max}} \rho(r, M) n(M) dM}{\int_{M_{min}}^{M_{max}} n(M) dM}, \quad (19)$$

where $n(M)$ is the halo mass function from Sheth & Tormen (1999), and $\rho(r, M)$ is the density profile of halos of mass M assumed to be in the NFW form (Navarro et al. 1995, 1996, 1997). We determine the concentration parameter c of halos following Zhao et al. (2009). The lower and upper limits of halo mass (M_{min} and M_{max}) are determined by matching the abundance of LRGs in our sample with that of dark matter halos given by the Sheth-Tormen mass function (Sheth & Tormen 1999). For this we have adopted the plausible assumption that the luminosity of a central galaxy is an increasing function of the mass of its halo.

We consider three redshifts which are $z = 0.21, 0.31$ and 0.41 , approximately the median redshifts of our LRG samples. The dark matter density within $0.3h^{-1}$ Mpc around LRGs of $-23.2 < M_{0.3g} < -21.8$ is predicted to increase by 24.6% from $z \sim 0.4$ to ~ 0.2 , and 12.1% from $z \sim 0.3$ and ~ 0.2 . The factor is 10.6% for $-21.8 < M_{0.3g} < -21.2$ from $z \sim 0.3$ to ~ 0.2 . It is clear that these predictions are much smaller when compared to the SDSS data. As can be seen from Figure 8, at $r_p < 0.3h^{-1}$ Mpc, the clustering amplitude changes by a factor of ~ 2 between $z \sim 0.4$ and ~ 0.2 , and by 20 - 50% between $z \sim 0.3$ and ~ 0.2 . This indicates that the observed evolution of galaxy clustering is caused not only by the evolution of the underlying dark matter, but also by the evolution of galaxies themselves. We note that, as our photometric sample is selected in r -band, the satellites may be biased to bluer galaxies as one goes to higher redshifts. We will come back to this point in future to explore the implications of our measurements presented in Figure 8.

Figure 9 shows the relative bias factor with respect to L^* galaxies as a function of satellite galaxy luminosity. Bias factors are calculated from the amplitude of $w_p(r_p)$, normalized by a $-21 < M_{0.1r} < -20$ sample and averaged over separations between $r_p = 2.5h^{-1}$ Mpc and $10h^{-1}$ Mpc. Curves in different colors refer to results from different LRG samples in Table 1. Since the photometric sample becomes somewhat incomplete for $L \lesssim L^*$ in the redshift range $0.36 < z < 0.46$, the bias factor for this sample (the green line in the figure) is normalized with respect to a $-21.0 < M_{0.1r} < -20.5$ sample instead of the $-21 < M_{0.1r} < -20$ one. Plotted in black triangles is the result of Li et al. (2006). Black dashed line is a fit obtained from the SDSS power spectrum by Tegmark et al. (2004). Relative bias factors at $0.16 < z < 0.26$ (Samples L1 and L2) are well consistent with those previous studies at all luminosities, except the bright end where our

measurement is slightly lower than that from Tegmark et al. (2004). Our bias factor measurements show that the luminosity dependence of galaxy clustering observed in the local Universe is very similar to that at intermediate redshift $z \sim 0.4$.

4.2. Projected density profiles and clustering of low- z galaxies

We have also measured $w_p(r_p)n$ and $w_p(r_p)$ for the eight volume limited samples of low-redshift galaxies listed in Table 2 and for different intervals of satellite luminosity. Since the volume covered by these spectroscopic samples is small due to their small redshift intervals, the $w_p(r_p)n$ and $w_p(r_p)$ measurements are more noisy than presented above for the LRG samples. In order to improve the S/N of our measurements, for a given satellite luminosity interval we combine the measurements for spectroscopic samples that share a same luminosity interval but span different redshift ranges. When doing the combination we weight each sample by its comoving volume divided by the variance of the measurement, in the same way as above when combining redshift sub-shells. The combined $w_p(r_p)n$ are plotted in Figure 10. We do not include independent plots for $w_p(r_p)$, which show behaviors very similar to $w_p(r_p)n$.

In Figure 11 we show the corresponding relative bias factors, based on data points over $1.9 \leq r_p \leq 10h^{-1}\text{Mpc}$. Results are plotted in blue, red and green curves for the three luminosity intervals of main galaxies. For comparison we also repeat the bias factors from previous work by Tegmark et al. (2004) and Li et al. (2006) based on purely spectroscopic samples which are similar to our samples of main galaxies. Our measurements are in good agreement with these previous determinations, validating our method for measuring galaxy clustering with photometric data.

Similar to what is found for LRGs at $z \sim 0.4$, the density profiles around galaxies in the local Universe also shows quite similar slope, independent of the luminosity of satellite galaxies. Unlike in the LRG samples, the galaxies in our low-redshift samples could be either centrals or satellites of their host halos. However, the fraction of satellites should be small as the spectroscopic objects in the SDSS are relatively bright (Zheng et al. 2007). Thus our conclusion made above for $z \sim 0.4$ more or less holds for the local Universe, that is, satellite galaxies of different luminosities are distributed within their halos in a similar way, if the halos host central galaxies of similar luminosity. This is consistent with previous studies (e.g. Vale & Ostriker 2004, 2006; Zheng et al. 2007) which have revealed a tight relation between central galaxy luminosity $\langle L_c \rangle$ and halo mass. Moreover, halo occupation distribution models usually assume galaxy distribution inside halos to trace their dark matter, based on studies of satellite distributions (e.g. Nagai & Kravtsov 2005; Macciò et al. 2006). Again, our results provide additional, clear evidence in support of this assumption.

5. Summary

Previous studies on galaxy clustering as a function of luminosity usually make use of spectroscopic galaxy catalogues. In this work we have developed a new method to measure projected galaxy number density profiles $w_p(r_p)n$ as well as projected correlation function $w_p(r_p)$ by cross-correlating spectroscopic galaxies with a deep photometric sample. In this method we are able to divide the photometric galaxies into luminosity intervals even when redshift information is unavailable. This enables us to measure $w_p(r_p)n$ and $w_p(r_p)$ as a function of not only the luminosity of the spectroscopic galaxy, but also that of the photometric galaxy. Since photometric samples are usually much deeper than spectroscopic ones, with our method one can explore the clustering of galaxies to fainter luminosities and higher redshifts than using a spectroscopic sample alone.

We have applied our method to a sample of 10^5 luminous red galaxy (LRGs) at $z \sim 0.4$ and a sample of about half a million galaxies at $z \sim 0.1$, both of which are cross-correlated with a deep photometric sample of about 20 million galaxies limited to $r = 21$. We have investigated the dependence of $w_p(r_p)n$ and $w_p(r_p)$ on galaxy luminosity and redshift, by dividing both spectroscopic and photometric galaxies into various luminosity intervals and different redshift ranges.

On dark matter halo scales (i.e. nonlinear scales), we find that our correlation functions and density profiles show quite similar slope to each other, independent of satellite galaxy luminosity. This indicates that satellite galaxies of different luminosities are distributed in a similar way within their host halos. This is true not only for LRGs at intermediate redshifts which are mostly central galaxies of their halos, but also for the general population of galaxies in the local Universe. Our result provides direct evidence supporting the assumption commonly-adopted in HOD modeling that the distribution of galaxies follows the dark matter distribution within their host halos.

On large scales, the relative bias factor of LRGs at $z \sim 0.4$ depends on luminosity in a manner similar to galaxies at $z \sim 0.1$, consistent with previous work based on autocorrelations of spectroscopic galaxies in the local Universe.

Eisenstein et al. (2005) measured mean overdensity around LRGs by cross-correlating the LRGs with 16 million photometric galaxies from SDSS using the deprojecting method described in an earlier work (Eisenstein 2003). However, it is hard to directly compare their measurements with ours due to the different luminosity and redshift ranges being considered.

Our method can be applied and extended to many important statistical studies of galaxy formation and evolution. By dividing galaxies into red and blue populations in the photometric sample according to their colors, we can quantify the evolution of the blue fraction of galaxies in clusters and groups from redshift 0.4 to the present day (i.e the Butcher-Oemler effect). Wide deep photometry surveys, such as Pan-Starrs (Kaiser 2004) and LSST (Tyson 2002), will be available in the next years. Combining such surveys with large spectroscopic samples, such as BOSS LRG sample will allow one to explore the clustering of galaxies from $z = 0$ to $z = 1$ for a wide range of luminosities. The WISE will produce an all-sky catalogs of infrared galaxies. By combining this

survey with SDSS samples with redshift, one can find how infrared galaxies are distributed relative to the network of optical galaxies with our method. We will study these and other important problems in our subsequent work.

This work is supported by NSFC (10821302, 10878001), by the Knowledge Innovation Program of CAS (No. KJCX2-YW-T05), by 973 Program (No. 2007CB815402), and by the CAS/SAFEA International Partnership Program for Creative Research Teams (KJCX2-YW-T23).

REFERENCES

- Abazajian, K. N., et al. 2009, *ApJS*, 182, 543
- Benson, A. J., Baugh, C. M., Cole, S., Frenk, C. S., & Lacey, C. G. 2000, *MNRAS*, 316, 107
- Berlind, A. A., & Weinberg, D. H. 2002, *ApJ*, 575, 587
- Blanton, M. R., et al. 2003, *ApJ*, 592, 819
- Blanton, M. R., Lin, H., Lupton, R. H., Maley, F. M., Young, N., Zehavi, I., & Loveday, J. 2003, *AJ*, 125, 2276
- Blanton, M. R., et al. 2005, *AJ*, 129, 2562
- Blanton, M. R., & Roweis, S. 2007, *AJ*, 133, 734
- Carlberg, R. G., Yee, H. K. C., Morris, S. L., Lin, H., Hall, P. B., Patton, D. R., Sawicki, M., & Shepherd, C. W. 2001, *ApJ*, 563, 736
- Chen, J., Kravtsov, A. V., Prada, F., Sheldon, E. S., Klypin, A. A., Blanton, M. R., Brinkmann, J., & Thakar, A. R. 2006, *ApJ*, 647, 86
- Coil, A. L., et al. 2004, *ApJ*, 609, 525
- Coil, A. L., Newman, J. A., Cooper, M. C., Davis, M., Faber, S. M., Koo, D. C., & Willmer, C. N. A. 2006, *ApJ*, 644, 671
- Coil, A. L., et al. 2008, *ApJ*, 672, 153
- Colless, M., et al. 2001, *MNRAS*, 328, 1039
- Cooray, A., & Sheth, R. 2002, *Phys. Rep.*, 372, 1
- Davis, M., & Peebles, P. J. E. 1983, *ApJ*, 267, 465
- Davis, M., et al. 2003, *Proc. SPIE*, 4834, 161

- de la Torre, S., et al. 2009, arXiv:0911.2252
- Eisenstein, D. J., et al. 2001, AJ, 122, 2267
- Eisenstein, D. J. 2003, ApJ, 586, 718
- Eisenstein, D. J., Blanton, M., Zehavi, I., Bahcall, N., Brinkmann, J., Loveday, J., Meiksin, A., & Schneider, D. 2005, ApJ, 619, 178
- Faber, S. M., et al. 2007, ApJ, 665, 265
- Firth, A. E., et al. 2002, MNRAS, 332, 617
- Goto, T., Yamauchi, C., Fujita, Y., Okamura, S., Sekiguchi, M., Smail, I., Bernardi, M., & Gomez, P. L. 2003, MNRAS, 346, 601
- Guo, Q., White, S., Li, C., & Boylan-Kolchin, M. 2010, MNRAS, 404, 1111
- Hamilton, A. J. S. 1993, ApJ, 417, 19
- Hamilton, A. J. S., & Tegmark, M. 2002, MNRAS, 330, 506
- Jing, Y. P., Mo, H. J., & Boerner, G. 1998, ApJ, 494, 1
- Jing, Y. P., & Boerner, G. 1998, ApJ, 503, 37
- Kaiser, N. 2004, Proc. SPIE, 5489, 11
- Kauffmann, G., Nusser, A., & Steinmetz, M. 1997, MNRAS, 286, 795
- Kazin, E. A., et al. 2010, ApJ, 710, 1444
- Larson, D., et al. 2010, arXiv:1001.4635
- Lake, G., & Tremaine, S. 1980, ApJ, 238, L13
- Le Fèvre, O., et al. 2005, A&A, 439, 845
- Li, C., Kauffmann, G., Jing, Y. P., White, S. D. M., Börner, G., & Cheng, F. Z. 2006, MNRAS, 368, 21
- Li, C., Jing, Y. P., Kauffmann, G., Börner, G., Kang, X., & Wang, L. 2007, MNRAS, 376, 984
- Lilly, S. J., et al. 2007, ApJS, 172, 70
- Lorrimer, S. J., Frenk, C. S., Smith, R. M., White, S. D. M., & Zaritsky, D. 1994, MNRAS, 269, 696
- Ma, C.-P., & Fry, J. N. 2000, ApJ, 543, 503

- Macciò, A. V., Moore, B., Stadel, J., & Diemand, J. 2006, MNRAS, 366, 1529
- Madgwick, D. S., et al. 2003, MNRAS, 344, 847
- Meneux, B., et al. 2006, A&A, 452, 387
- Meneux, B., et al. 2008, A&A, 478, 299
- Meneux, B., et al. 2009, A&A, 505, 463
- Nagai, D., & Kravtsov, A. V. 2005, ApJ, 618, 557
- Navarro, J. F., Frenk, C. S., & White, S. D. M. 1997, ApJ, 490, 493
- Navarro, J. F., Frenk, C. S., & White, S. D. M. 1996, ApJ, 462, 563
- Navarro, J. F., Frenk, C. S., & White, S. D. M. 1995, MNRAS, 275, 720
- Norberg, P., et al. 2002, MNRAS, 332, 827
- Norberg, P., et al. 2001, MNRAS, 328, 64
- Okumura, T., Jing, Y. P., & Li, C. 2009, ApJ, 694, 214
- Peacock, J. A., & Dodds, S. J. 1996, MNRAS, 280, L19
- Peacock, J. A., & Smith, R. E. 2000, MNRAS, 318, 1144
- Phillipps, S., & Shanks, T. 1987, MNRAS, 229, 621
- Phleps, S., Peacock, J. A., Meisenheimer, K., & Wolf, C. 2006, A&A, 457, 145
- Reid, B. A., & Spergel, D. N. 2009, ApJ, 698, 143
- Ross, A. J., Brunner, R. J., & Myers, A. D. 2007, ApJ, 665, 67
- Sales, L., & Lambas, D. G. 2005, MNRAS, 356, 1045
- Scoccimarro, R., Sheth, R. K., Hui, L., & Jain, B. 2001, ApJ, 546, 20
- Seljak, U. 2000, MNRAS, 318, 203
- Seljak, U., & Zaldarriaga, M. 1996, ApJ, 469, 437
- Shepherd, C. W., Carlberg, R. G., Yee, H. K. C., Morris, S. L., Lin, H., Sawicki, M., Hall, P. B.,
& Patton, D. R. 2001, ApJ, 560, 72
- Sheth, R. K., & Tormen, G. 1999, MNRAS, 308, 119
- Tegmark, M., Hamilton, A. J. S., & Xu, Y. 2002, MNRAS, 335, 887

- Tegmark, M., et al. 2004, *ApJ*, 606, 702
- The SDSS Collaboration, et al. 2010, arXiv:1005.2413
- Tinker, J. L., Weinberg, D. H., Zheng, Z., & Zehavi, I. 2005, *ApJ*, 631, 41
- Tyson, J. A. 2002, *Proc. SPIE*, 4836, 10
- Vader, J. P., & Sandage, A. 1991, *ApJ*, 379, L1
- Vale, A., & Ostriker, J. P. 2006, *MNRAS*, 371, 1173
- Vale, A., & Ostriker, J. P. 2004, *MNRAS*, 353, 189
- Wang, L., & Jing, Y. P. 2010, *MNRAS*, 402, 1796
- Westra, E., Geller, M. J., Kurtz, M. J., Fabricant, D. G., Dell’Antonio, I., Astrophysical Observatory, S., & University, B. 2010, arXiv:1006.2823
- Yang, X., Mo, H. J., & van den Bosch, F. C. 2003, *MNRAS*, 339, 1057
- York, D. G., et al. 2000, *AJ*, 120, 1579
- Zaldarriaga, M., & Seljak, U. 2000, *ApJS*, 129, 431
- Zaldarriaga, M., Seljak, U., & Bertschinger, E. 1998, *ApJ*, 494, 491
- Zehavi, I., et al. 2002, *ApJ*, 571, 172
- Zehavi, I., et al. 2005, *ApJ*, 621, 22
- Zehavi, I., et al. 2005, *ApJ*, 630, 1
- Zhao, D. H., Jing, Y. P., Mo, H. J., Börner, G. 2009, *ApJ*, 707, 354
- Zheng, Z., et al. 2005, *ApJ*, 633, 791
- Zheng, Z., Coil, A. L., & Zehavi, I. 2007, *ApJ*, 667, 760

Table 1. LRG samples selected according to luminosity and redshift

SAMPLE (1)	$M_{0.3g}$ (2)	z (3)	Num. of galaxies (4)	Sub-shell information	
				Num. of sub-shells (5)	Δz_{sub} (6)
L1	(-23.2,-21.8)	(0.16,0.26)	5592	5	0.02
L2	(-21.8,-21.2)	(0.16,0.26)	16832	5	0.02
L3	(-23.2,-21.8)	(0.26,0.36)	11647	5	0.02
L4	(-21.8,-21.2)	(0.26,0.36)	26301	5	0.02
L5	(-23.2,-21.8)	(0.36,0.46)	17502	5	0.02

Table 2. Low-redshift volume-limited samples of galaxies selected by luminosity and redshift

SAMPLE (1)	$M_{0.1r}$ (2)	z (3)	Num. of galaxies (4)	Sub-shell information	
				Num. of sub-shells (5)	Δz_{sub} (6)
VL1	(-21.0,-20.2)	(0.03,0.07)	20553	10	0.004
VL2	(-23.0,-21.0)	(0.03,0.07)	5879	10	0.004
VL3	(-21.0 -20.2)	(0.07,0.11)	63694	5	0.008
VL4	(-23.0 -21.0)	(0.07,0.11)	19138	5	0.008
VL5	(-23.0,-21.0)	(0.11,0.15)	40226	4	0.01
VL6	(-23.0,-21.9)	(0.11,0.15)	2330	4	0.01
VL7	(-23.0,-21.9)	(0.15,0.19)	3935	4	0.01
VL8	(-23.0,-21.9)	(0.19,0.23)	5268	4	0.01

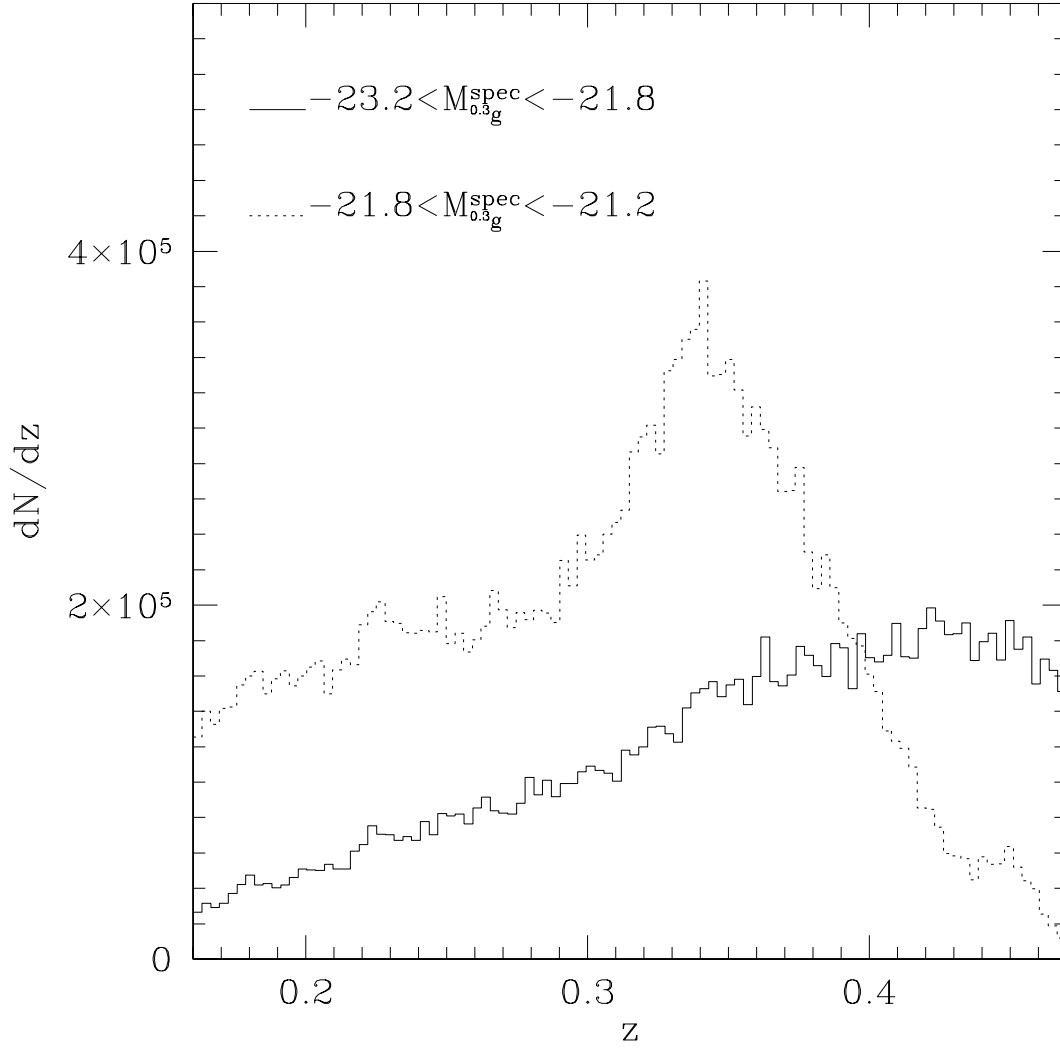


Fig. 1.— redshift distribution of central LRGs with two luminosity cuts as shown by the legend, in which the g-band absolute magnitude $M_{0.3g}$ is K+E corrected to $z = 0.3$. The upper index “spec” in the legend is to emphasize that the absolute magnitude is for spectroscopic main galaxy sample, in order to distinguish that for the photometric sample in other plots.

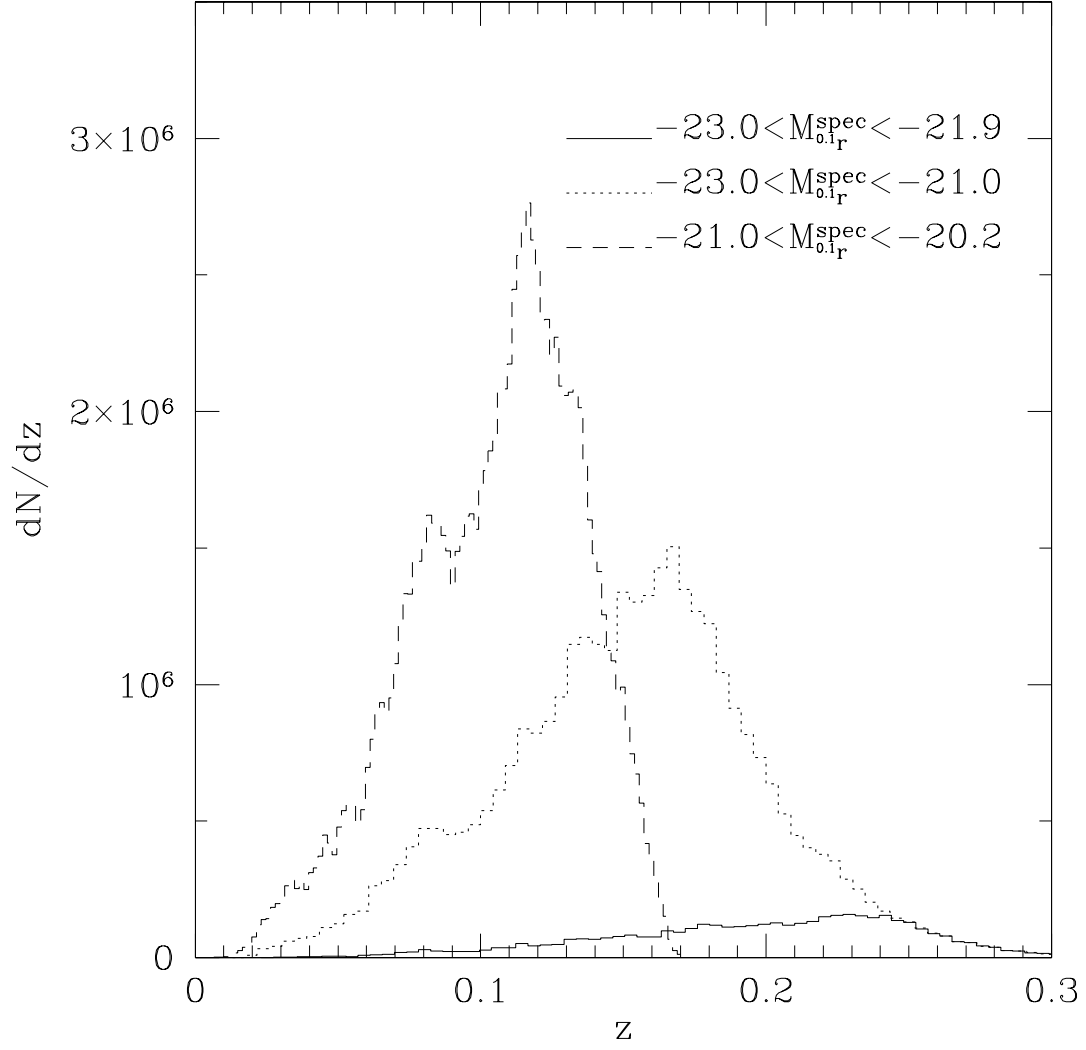


Fig. 2.— redshift distribution of spectroscopic main galaxies with different luminosity cuts as shown by the legend. The r-band absolute magnitude $M_{0.1g}$ is K+E corrected to $z = 0.1$.

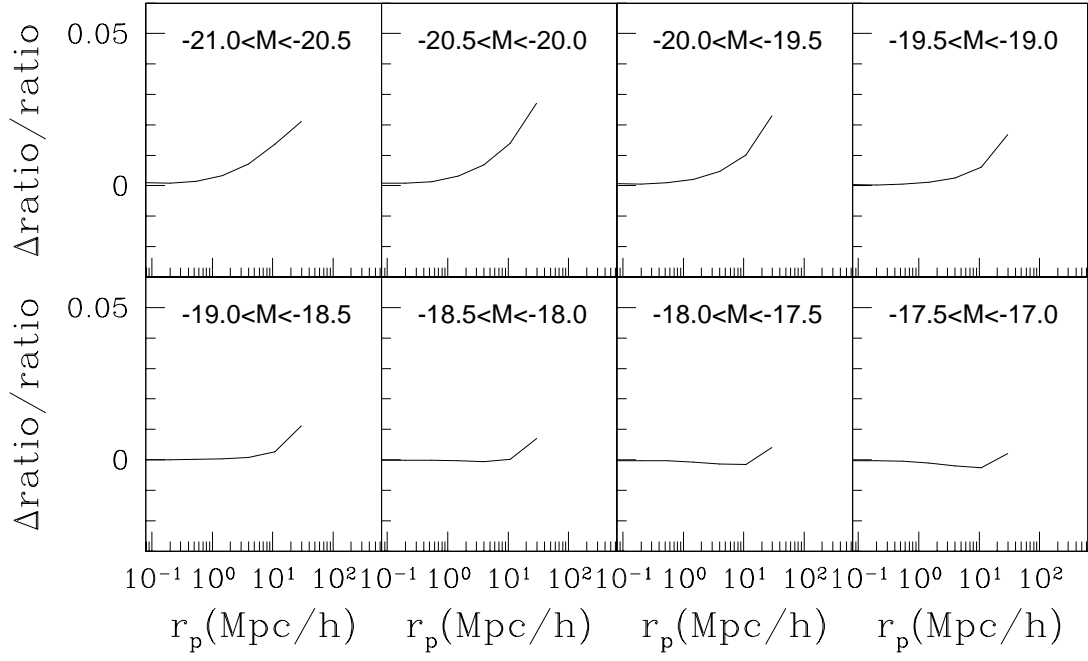


Fig. 3.— The relative difference between the ratio calculated from $w(\theta)$ divided by $w_p(r_p)$ directly and that calculated from Eqn. (13). In this plot, we assume spectroscopic galaxies are at $0.07 < z < 0.078$. The luminosity bins for photometric galaxies are shown by legend of each sub panel.

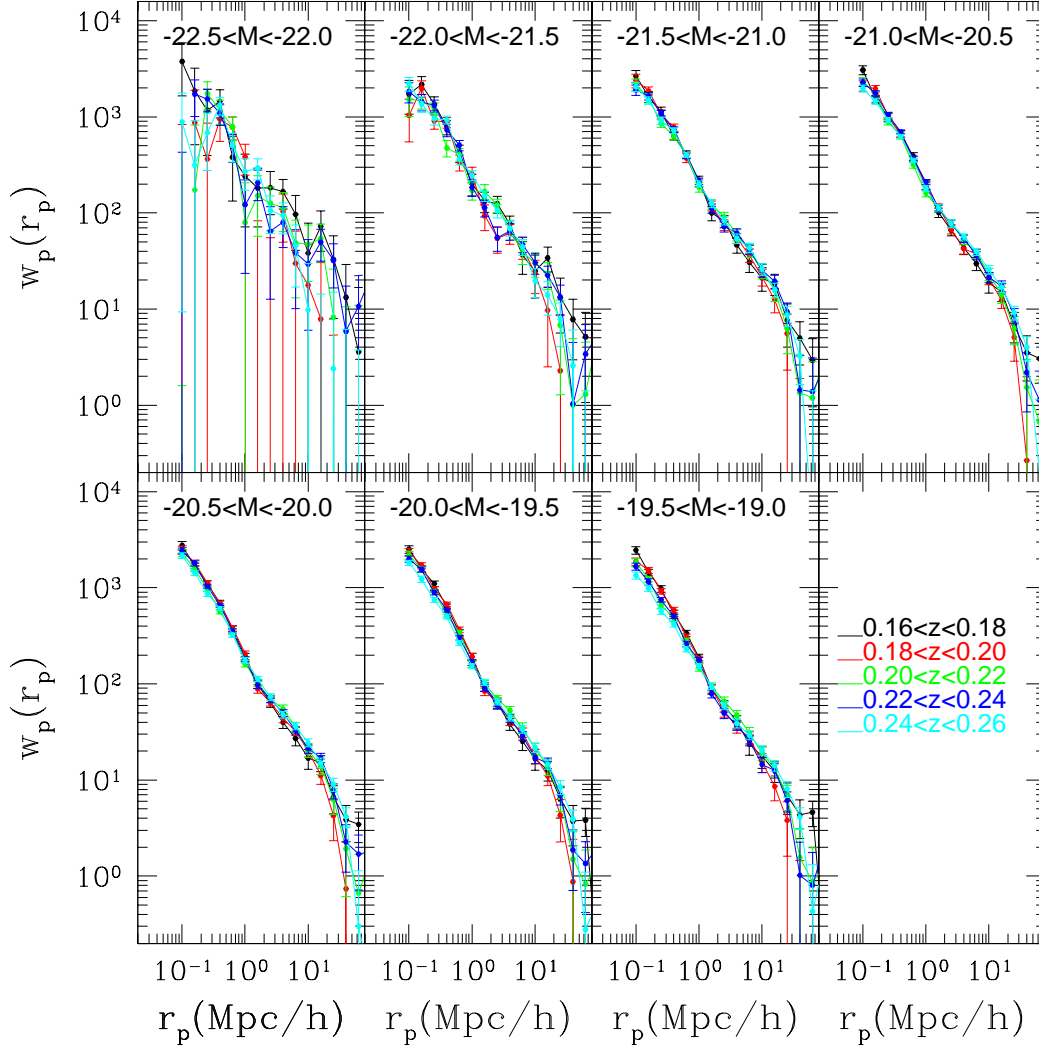


Fig. 4.— Projected cross-correlation function $w_p(r_p)$ for redshift sub-shells of the L1 LRG sample in Table 1, estimated by cross correlating each sub-shell with photometric galaxies in different luminosity intervals as indicated in each panel. Different lines are for different sub-shells of which the redshift ranges are indicated in the bottom-right panel.

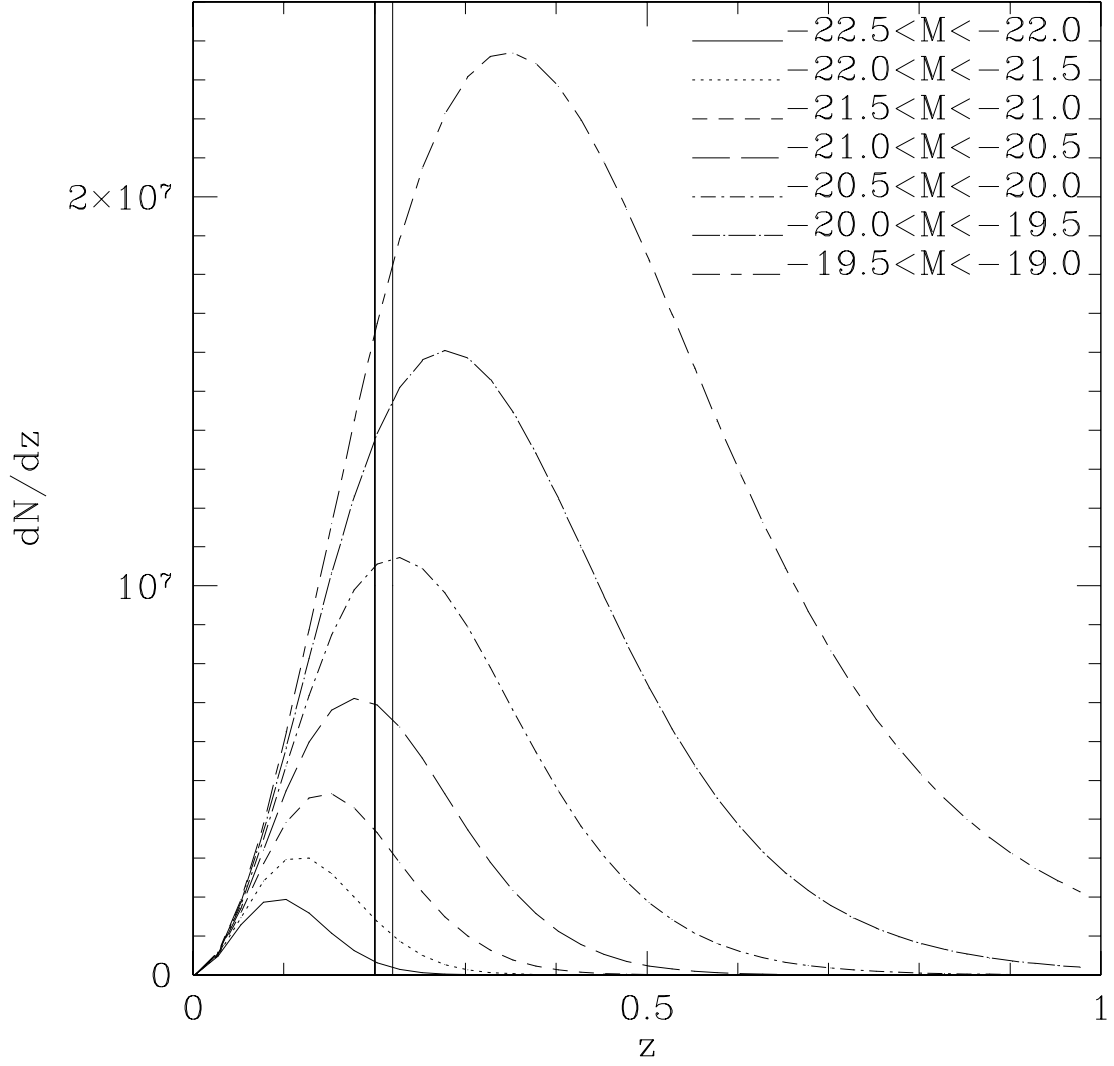


Fig. 5.— Redshift distribution predicted by the luminosity function of B03 for photometric galaxies that are expected to fall in the indicated luminosity intervals if they were located in the redshift range $0.2 < z < 0.22$, as indicated by the two vertical lines.

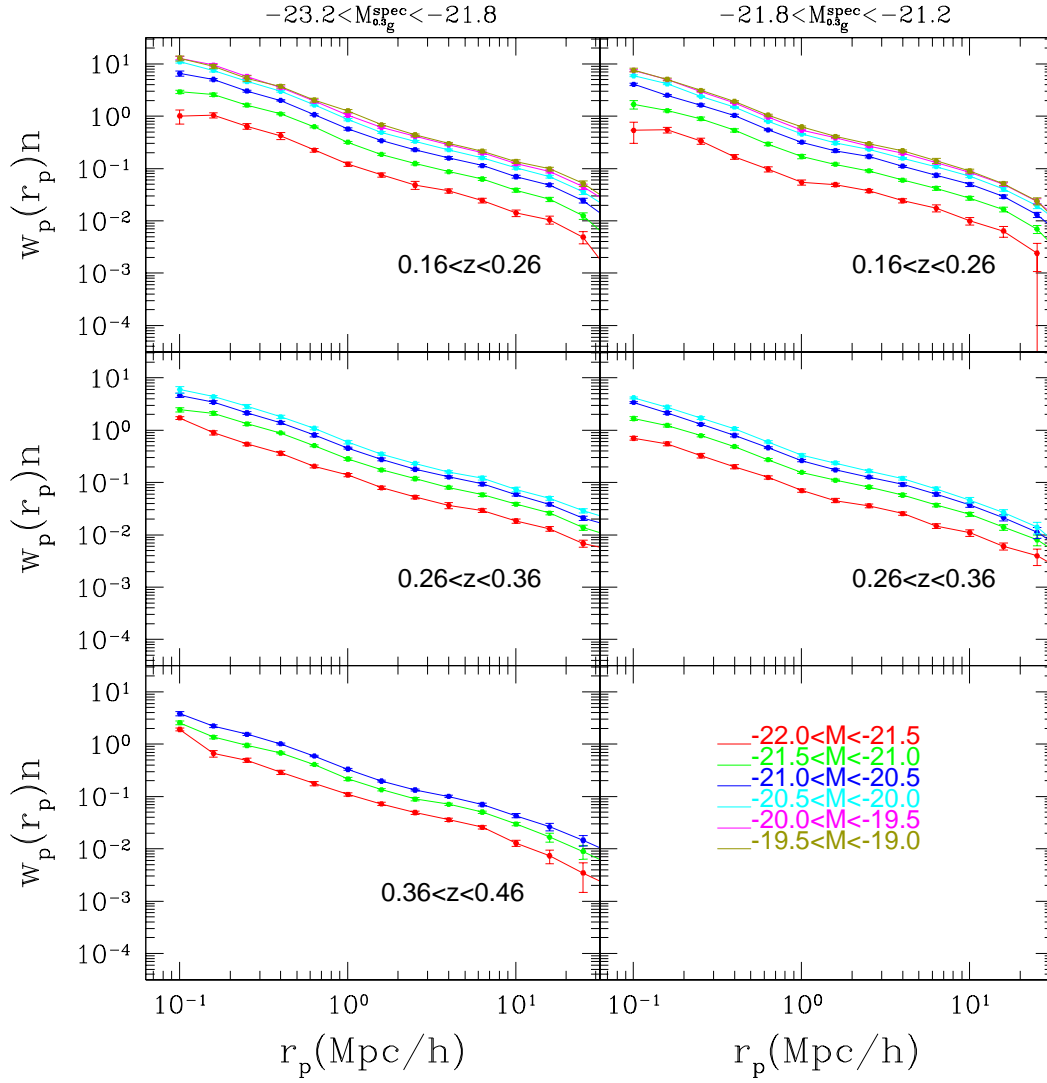


Fig. 6.— Projected density profile $w_p(r_p)n$ in units of $Mpc^{-2}h^2$ surrounding LRGs with different luminosities (indicated above the figure) and redshifts (indicated in each panel), as traced by galaxies of different luminosities (shown in different lines in each panel).

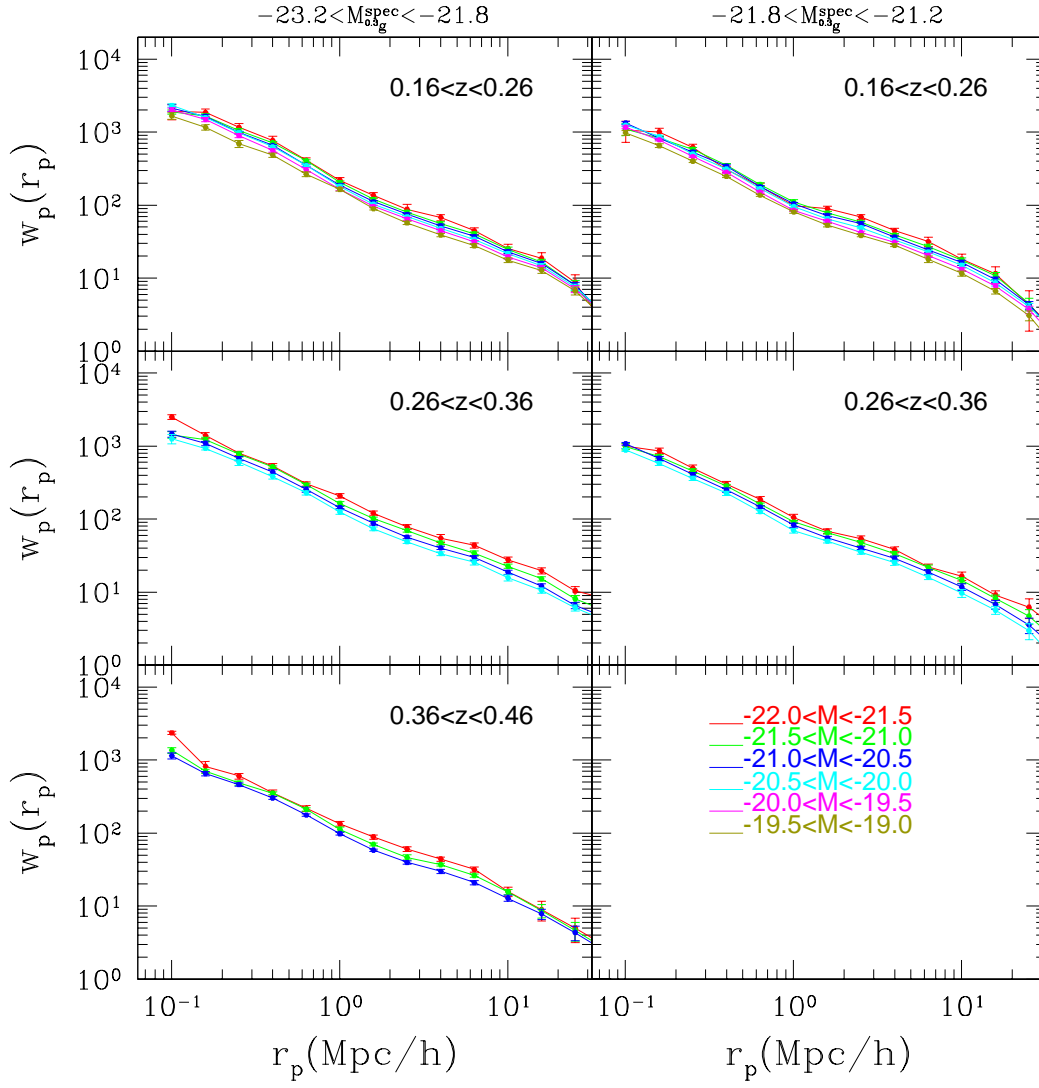


Fig. 7.— Projected cross-correlation function $w_p(r_p)$ measured for the same set of LRG samples and the same intervals of satellite luminosity as in the previous figure.

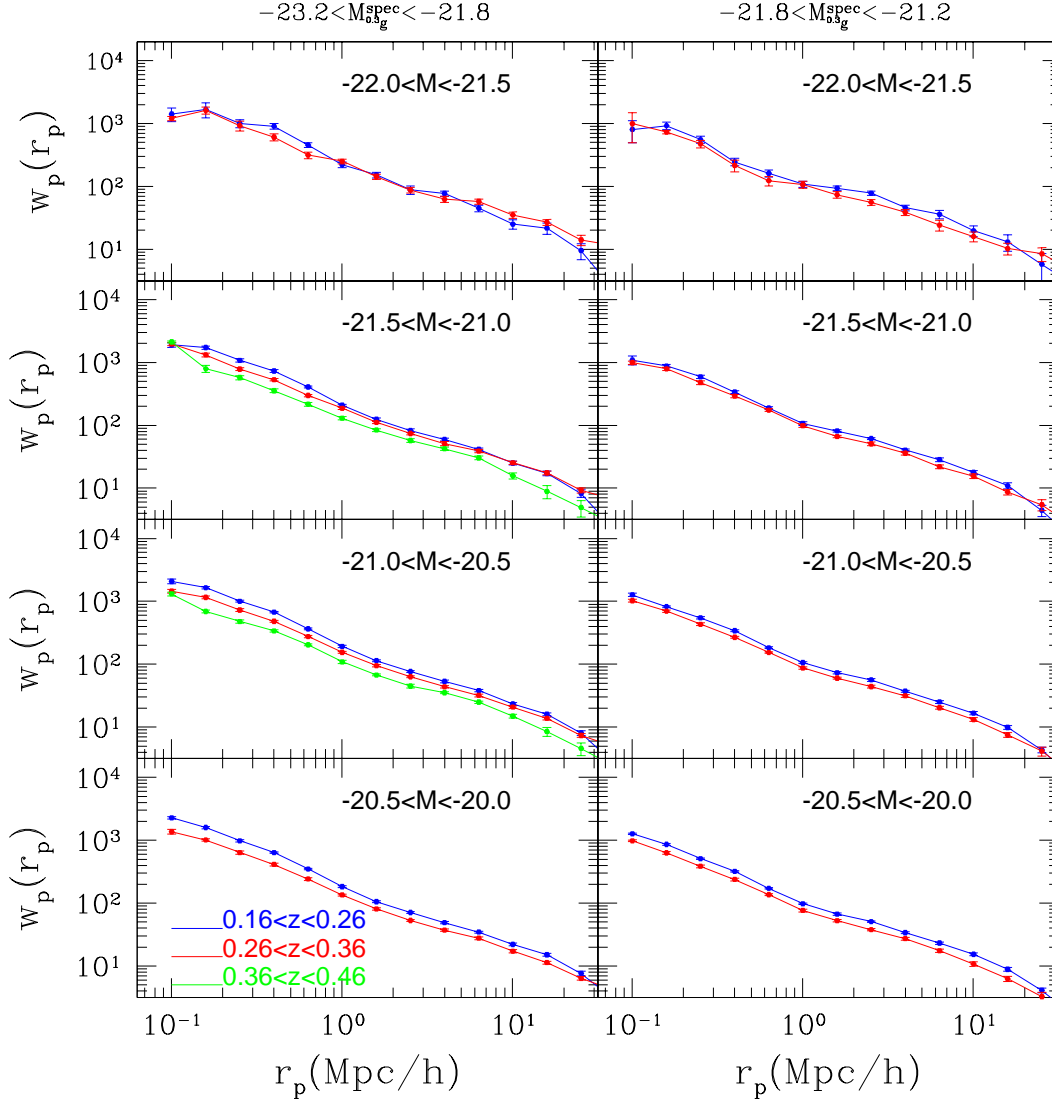


Fig. 8.— Each panel shows a comparison among $w_p(r_p)$ at different redshift but with the same luminosity range for photometric and spectroscopic galaxies. The luminosity range is shown in the legend of each panel. Different color of lines stand for different redshift bin, as shown by color legends in the bottom left panel. The two columns refer to results obtained with LRG samples with different luminosity cut, as shown by the top legend above the figure. We have considered E-correction in this figure.

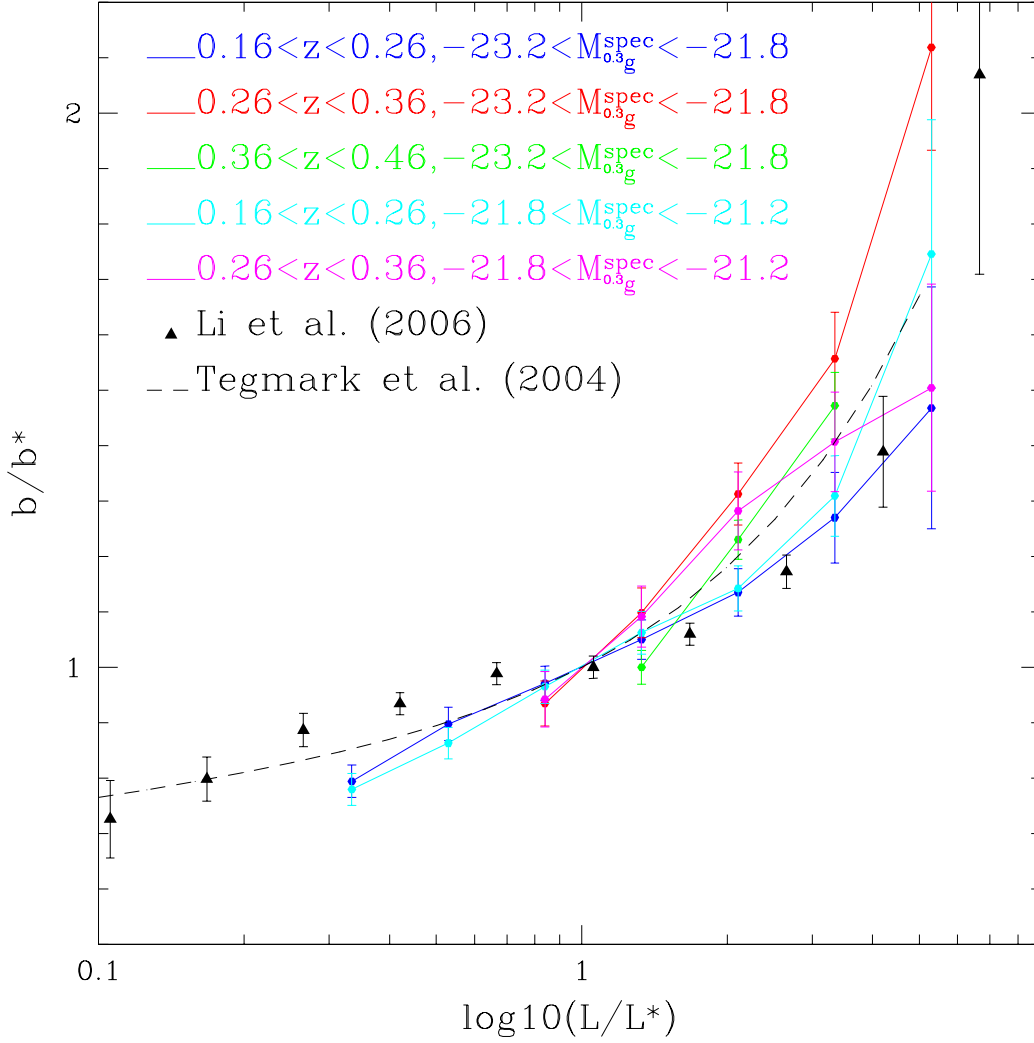


Fig. 9.— Relative bias factor with respect to L^* and its dependence on luminosity obtained from the cross correlation between LRGs and photometric catalogue. Bias factors are calculated from the amplitude of $w_p(r_p)$ averaged between $r = 2.5h^{-1}Mpc$ and $r = 10.0h^{-1}Mpc$, normalized by a $-21 < M < -20$ photometric sample. But notice for the $0.36 < z < 0.46$ bin, the photometric catalogue becomes incomplete when $M > -20.5$, so we calculate the relative bias factor with respect to a $-21.0 < M < -20.5$ photometric sample. Different color of curves refer to results obtained with different LRG subsamples, as shown by the color legends. Black triangles and the black dashed line stand for previous result of Li et al. (2006) and a fit obtained from SDSS power spectrum, which is $b/b^* = 0.85 + 0.15L/L^* - 0.04(M - M^*)$ (Tegmark et al. 2004).

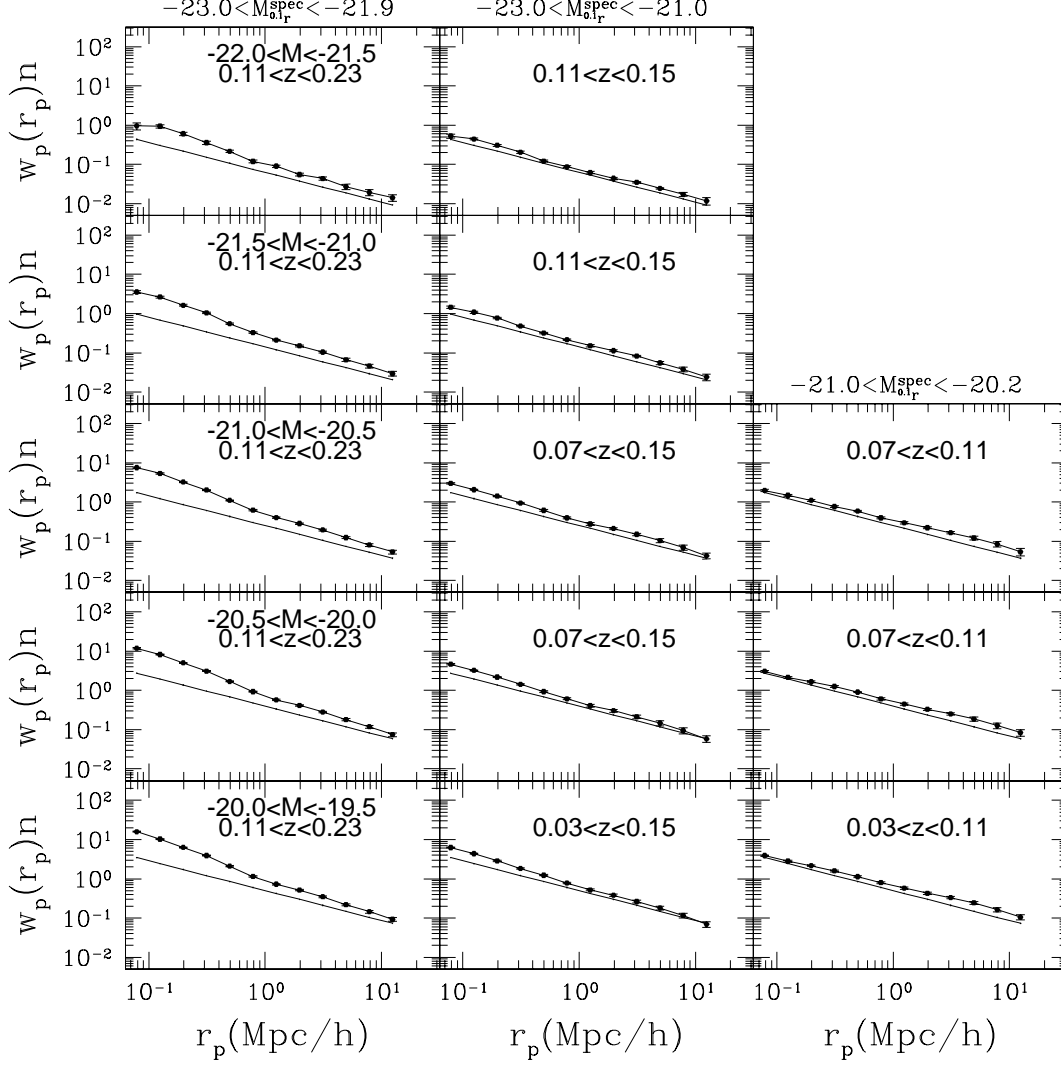


Fig. 10.— Each panel shows the averaged $w_p(r_p)n$ over different redshift bins in Table 2. Redshift bins to do the average in each single panel are with the same magnitude cut for both spectroscopic main galaxies and satellite galaxies. Panels in each column refer to results with the same spectroscopic main galaxy luminosity cut, as shown by the top legends above the figure. Panels in the same row are results with the same luminosity range of photometric galaxies, as shown by legends in the most left panels. The redshift range over which we doing average is shown by legends in each panel. The solid black straight line is for guiding our eye, which has the same slope in each different panel.

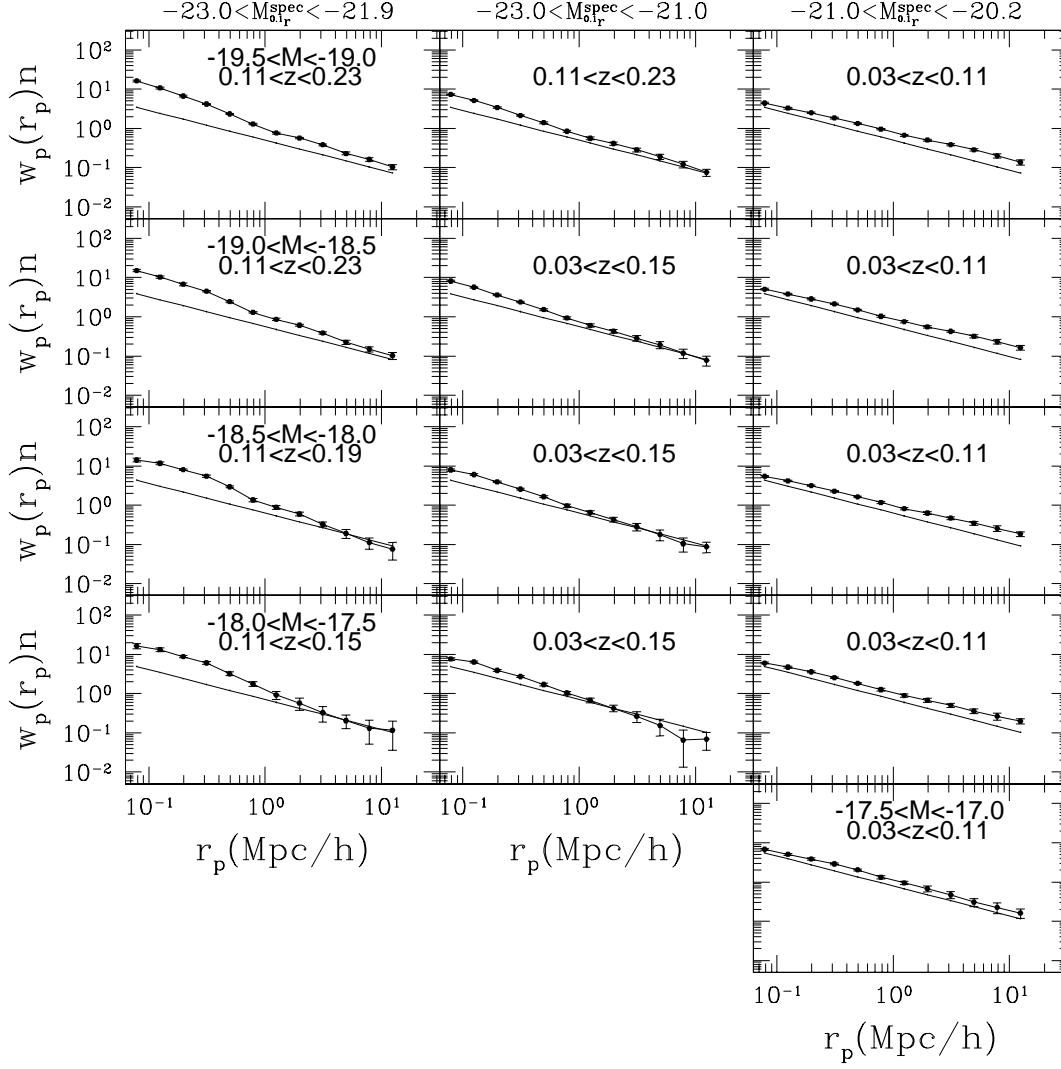


Fig. 10.— Continued...

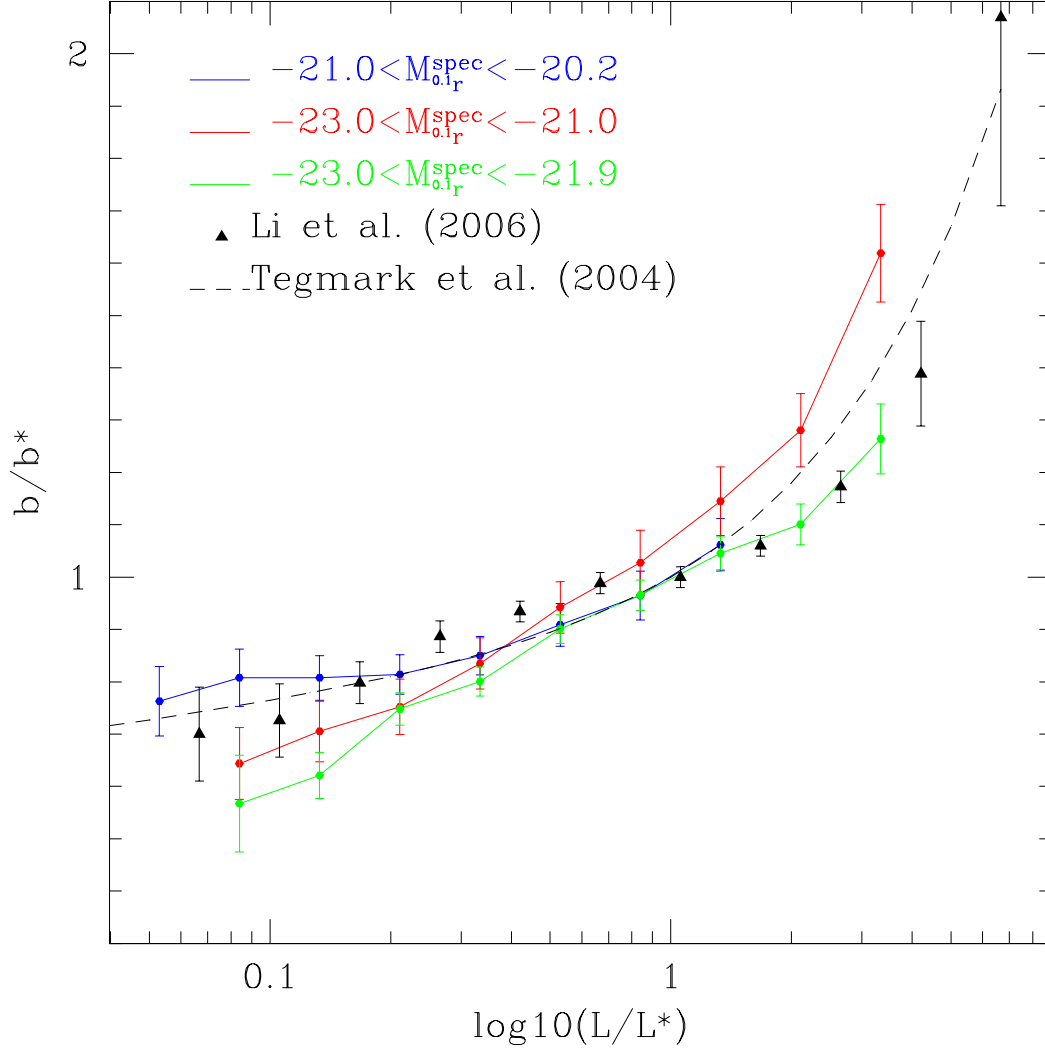


Fig. 11.— Relative bias factor dependence on luminosity similar as in figure 9. But calculated from the spectroscopic main galaxy part. Bias factors are calculated by the amplitude of $w_p(r_p)$ averaged between $r = 1.9h^{-1}Mpc$ and $r = 10.0h^{-1}Mpc$, normalized by a $-21 < M < -20$ photometric sample.